Passive instability control by a heat exchanger in a combustor with non-uniform temperature

Aswathy Surendran and Maria A. Heckl

Abstract

Thermoacoustic instabilities, caused by the feedback between unsteady heat release and pressure perturbations, are characterised by large amplitude pressure oscillations. These oscillations, if unchecked and uncontrolled, pose a great threat to combustion systems. One strategy to mitigate them is by the use of cavity backed acoustic liners (perforated plates). In this study, we consider a generic combustor configuration: a quarter-wave resonator (1-D, one end open and the other end closed) containing a compact heat source and heat exchanger tube row. The aim is to use the heat exchanger tube row as the acoustic damper. The heat exchanger tubes are simulated using an array of thin rods with rectangular cross-section and having a bias flow through the gaps between the rods. When placed near the closed end of the resonator, these rods behave like a cavity-backed slit-plate/an acoustic liner. We derive the characteristic equation for the complex eigenfrequencies of this set-up. From the growth rates (imaginary parts of the eigenfrequencies), we construct stability maps for various system parameter combinations. Preliminary results show that increasing the bias flow through the slits tends to stabilise the system.

Introduction

Thermoacoustic instabilities, if unchecked and uncontrolled in combustors, can cause catastrophic damage to the hardware. These instabilities arise due to the existence of a positive feedback between the unsteady heat release and the acoustic pressure oscillations. It is important to develop mitigation strategies to predict and prevent these instabilities. One such strategy that gained popularity in recent years is the use of cavity backed acoustic liners in combustors.

Researchers have proved both theoretically and experimentally, that acoustic liners when backed by a cavity could effectively damp acoustic waves. These liners are usually plates with sharp edged circular/ elliptical perforations. The presence of a bias flow in these perforations induce vortex shedding from the sharp edges, causing the vortices to act as acoustic sinks. Bechert (1980) quantitatively measured this mechanism of sound absorption in a jet flow. Howe (1979) derived expressions for the absorptive properties of perforated plates in unsteady high Reynolds number flows, and Hughes and Dowling (1990) evaluated the absorption properties of cavity backed perforated plates, with bias flow. Tran et al. (2009) experimentally verified the applicability of this absorption mechanism to stabilise their combustor. Theoretical analysis and stability predictions of Tran's combustor were carried out by Heckl and Kosztin (2013).

In the present study, we aim to stabilise an existing unstable mode of a generic combustion system with non-uniform temperature, using a heat exchanger. The heat exchanger consists of an array of tubes and these tubes are simulated as thin sharp edged rods with rectangular cross-section, enabling us to use the approximation of a slit-plate. The combustor is treated as a quarter-wave resonator

with a heat source, open at one end and closed at the other, and when the heat exchanger tubes are placed close to the closed end, they behave like a cavity-backed slit-plate or an acoustic liner. Dowling and Hughes (1992) have shown, both numerically and experimentally, that the sound waves incident on a slit-plate backed by cavity will be completely absorbed, provided the cavity length and bias flow velocity are chosen appropriately. Surendran and Heckl (2015) developed a theoretical model for this absorption method and demonstrated that it can stabilise an unstable mode in a combustor with uniform temperature distribution and a compact heat source. This study aims to extend the latter work to account for a non-uniform temperature regime and a more general heat release law.

Description of model

The combustion system studied is as shown in Fig. 1. It consists of a quarter-wave resonator, open at the upstream end ($x = 0$) and having a reflection coefficient $R_0 = -1$. The heat source is located at a distance l_f from the upstream end, dividing the resonator into two regions: a cold upstream region (Region 1) and a hot downstream region (Region 2). The speeds of sound ($c_{1,2}$) and mean temperatures ($T_{1,2}$) are uniform in both regions. The slit-plate (also referred to as acoustic liner in the present paper) simulating the heat excha-

School of Computing and Mathematics, Keele University, Staffordshire, UK

Corresponding author:
Aswathy Surendran, School of Computing and Mathematics, Keele University, Staffordshire, ST55BG, UK.
Email: a.surendran@keele.ac.uk

nger is located at the location $x = L$. The slit-plate has a bias flow through the gaps, denoted by its Mach number, M. The downstream end of the combustor is equipped with a rigid piston, enabling us to vary the distance between the slit-plate and the piston. This distance is referred to as the cavity length (l_c).
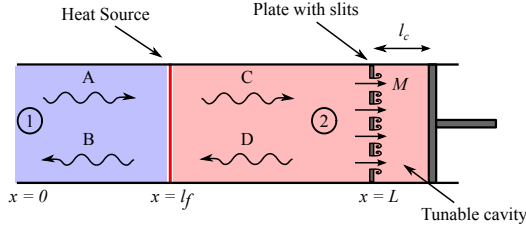
Figure 1. Schematic of the combustion system

Acoustic Field

The acoustic field within the combustor is modelled as one-dimensional acoustic waves propagating perpendicular to the rods (normal incidence), as shown in Fig. 1. For the present study, we ignore the heat transfer between the rods and the surrounding fluid, i.e. air. The acoustic pressure and velocity fields inside the resonator are,

Region 1:

$$\hat{p}_1(x) = Ae^{ik_1(x-l_f)} + Be^{-ik_1(x-l_f)} \qquad 0 < x < l_f \tag{1}$$

$$\hat{u}_1(x) = \frac{1}{\rho_1 c_1}\left\{ Ae^{ik_1(x-l_f)} - Be^{-ik_1(x-l_f)} \right\} \quad 0 < x < l_f \tag{2}$$

Region 2:

$$\hat{p}_2(x) = Ce^{ik_2(x-l_f)} + De^{-ik_2(x-l_f)} \qquad l_f < x < L \tag{3}$$

$$\hat{u}_2(x) = \frac{1}{\rho_2 c_2}\left\{ Ce^{ik_2(x-l_f)} - De^{-ik_2(x-l_f)} \right\} \quad l_f < x < L, \tag{4}$$

where $\hat{p}$ and $\hat{u}$ are the acoustic pressure and acoustic velocity respectively, A, B, C and D are the pressure amplitudes to be determined and $k_{1,2} = \omega/c_{1,2}$ is the wave number. The subscripts 1 and 2 indicate the regions within the resonator. The factor of $e^{-i\omega t}$ is omitted throughout the analysis.

Generic Heat Release Law

The heat source is assumed to be compact, planar and confined to an infinitesimally thin region at $x = l_f$. For the heat release rate ($\hat{Q}$), we have adopted the generic heat release law by Heckl and Kosztin (2013), where the heat release rate depends on both the instantaneous velocity fluctuations $u(t)$ as well as the time lagged velocity fluctuations $u(t - \tau)$ at the location l_f. It is given by:

$$\hat{Q}(\omega) = \alpha\left[n_1\hat{u}(l_f)e^{i\omega\tau} - n_0\hat{u}(l_f) \right] \tag{5}$$

$$\hat{Q}(\omega) = \frac{\alpha(A - B)}{\rho_1 c_1}\left[n_1 e^{i\omega\tau} - n_0 \right] \tag{6}$$

where α is a factor relating the local and global heat release rates and n_1 and n_0 are non-dimensional coefficients called coupling coefficients.

Cavity backed Slit-plate

The heat exchanger is modelled as an array of thin rods, spaced a distance d apart, having rectangular cross sections (Fig. 2). Therefore, we can treat this array as a plate with slits of width $2s$. A pressure difference across the slit-plate creates a bias flow of Mach number M through the slits, causing vortex shedding. These vortices act as acoustic dampers. In the model by Dowling and Hughes (1992), the transmission and reflection coefficients of a slit-plate with bias flow were derived as,

$$T_{sp} = \rho\omega\dot{V}/(kd) \tag{7}$$

$$R_{sp} = 1 - \rho\omega\dot{V}/(kd) \tag{8}$$

with

$$\frac{\rho\omega\dot{V}}{kd} = \frac{i\pi\nu/(2\kappa sM)}{i\pi\nu/(2\kappa sM) - \ln(\pi\nu) + \ln 2/\Phi} \tag{9}$$

and

$$\Phi = 1 - \frac{1}{\kappa s \ln 2}\left\{ \frac{\pi I_0(\kappa s)e^{\kappa s} + 2i\sinh(\kappa s)K_0(\kappa s)}{\pi e^{-\kappa s}\left[I_1(\kappa s) + \frac{I_0(\kappa s)}{\kappa s \ln 2} \right] + 2i\sinh(\kappa s)\left[\frac{K_0(\kappa s)}{\kappa s \ln 2} - K_1(\kappa s) \right]} \right\}. \tag{10}$$

The subscript *sp* refers to slit-plate and $\dot{V}$ is the perturbation volume flux through the slit. $\nu = 2s/d$ is the open area ratio, $\kappa s = \omega s/U$ is the Strouhal number, U is the bias flow velocity, and I_m and K_m are the modified Bessel functions of order m. The readers are advised to refer to Dowling and Hughes (1992) for further details. The rigid wall backing the plate is at a distance l_c from the slit-plate. The effective reflection coefficient, R_L, of the cavity-backed slit-plate is given by (Surendran and Heckl (2014)),

$$R_L = R_{sp} + \frac{T_{sp}^2 e^{2ik_2 l_c}}{1 - R_{sp}e^{2ik_2 l_c}}. \tag{11}$$
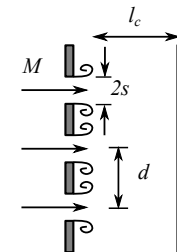
Figure 2. Geometry of the slit plate

In situations where the acoustic liner is non-dissipative, $|T_{sp}|^2 + |R_{sp}|^2 = 1$ for slit-plate with bias flow (Howe

(1998)) and $|R_L|^2 = 1$ for a cavity-backed slit-plate. When the liner is dissipative, these equations do not hold, instead $|T_{sp}|^2 + |R_{sp}|^2 < 1$ and $|R_L|^2 < 1$. This enables us to define a quantity known as the absorption coefficient (Δ) of the liner, which is the ratio of the acoustic energy dissipated/absorbed by the liner to the incident acoustic energy.

$$\Delta_{sp} = 1 - |T_{sp}|^2 - |R_{sp}|^2, \tag{12}$$

$$\Delta_L = 1 - |R_L|^2. \tag{13}$$

From Eqs. (7)-(13), we can observe that the absorption coefficient Δ is influenced by the bias flow Mach number (M), the angular frequency of the incident wave (ω) and the open area ratio (ν), for both the slit-plate with bias flow and the cavity-backed slit-plate with bias flow. The cavity-backed slit-plate has an additional influence from the cavity length (l_c). The influence of these parameters on the $|R|$ and Δ of the slit-plate and the cavity-backed slit-plate are shown in Figs. 3 - 6. Figure 3 shows the reflection coefficient and absorption coefficient for a slit-plate (Figs. 3 (a) and (b)) and cavity-backed slit-plate (Figs. 3 (c) and (d)), as functions of

Mach number, M, for 3 fixed frequency values: $f = 60$, 120 and 170Hz. From Fig. 3 (a) and (b), we observe that the $|R_{sp}|$ increases with M, whereas the Δ_{sp} increases initially with M, reaches a maximum of 0.5 and then decreases. Across frequencies, we observe that $|R_{sp}|$ and Δ_{sp} are almost constant values i.e., the slit-plate behaves almost similarly for the frequencies considered. But, when we have a cavity-backed slit-plate, the $|R|$ and Δ have different behavioural trends with M, when compared to a slit-plate (Figs. 3(c) and (d)). Figure 3 (c) shows the reflection coefficient $|R_L|$ as a function of M. As M increases, the $|R_L|$ decreases, reaches a minimum and then increases. The absorption coefficient Δ_L, on the other hand, exhibits the opposite behaviour. In addition to this, the cavity-backed slit-plate behaves differently across frequencies. For a constant M value and increasing frequency, $|R_L|$ decreases, while Δ_L increases. These results can also be deduced from Fig. 4, which shows $|R|$ and Δ of a slit-plate (Figs. 4 (a) and (b)) and a cavity-backed slit-plate (Figs. 4 (c) and (d)) as functions of frequency for 4 fixed M : $M = 0.001$, 0.015, 0.05 and 0.1.
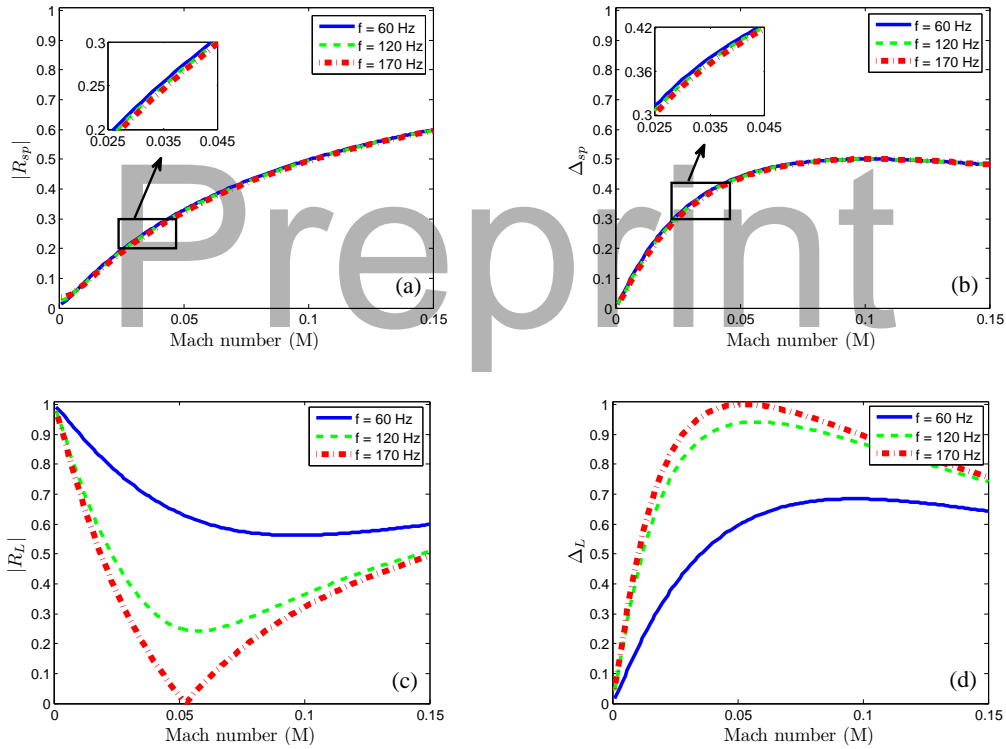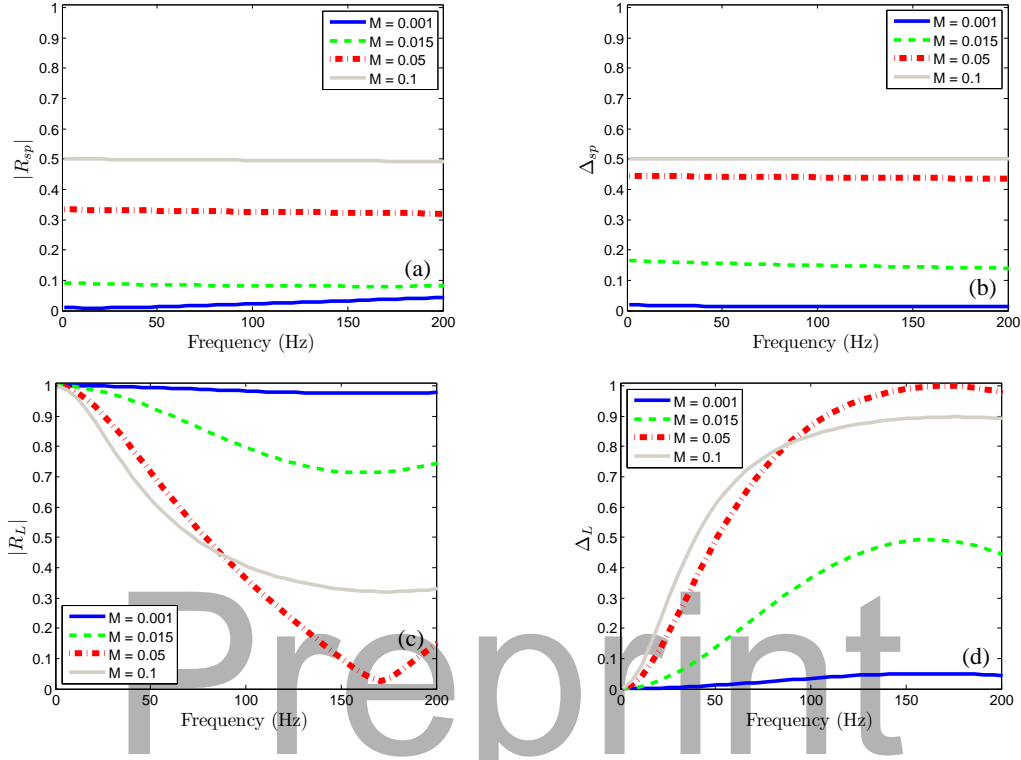

Figure 3. Reflection coefficient and absorption coefficient of slit-plate ((a) and (b)) and cavity-backed slit-plate ((c) and (d)) as a function of Mach number, for fixed frequency values and $\nu = 0.1$. For (c) and (d), $l_c = 0.5$m.

Figure 4 (a) and (b) reinforces the conclusions we drew from Fig. 3 (a) and (b) i.e., $|R_{sp}|$ and Δ_{sp} are almost constants across frequencies for the different M values. In Fig. 4 (c) and (d), we notice that, for the cavity-backed slit-plate, the $|R_L|$ decreases with increasing f, attains a minimum and then increases, while Δ_L increases initially, reaches a maximum and then decreases. Across M values, $|R_{sp}|$ and Δ_{sp} increases with increasing M (Fig. 4 (a) and (b)), whereas $|R_L|$ decreases with increasing M and Δ_L increases with increasing M (Fig. 4 (c) and (d)).

In order to achieve complete absorption of an acoustic wave of frequency f, incident normal to the cavity backed slit-plate, l_c must be chosen such that $l_c = c/(4f)$ (Dowling and Hughes (1992)). This means that l_c must be a quarter of the wavelength of the incoming acoustic wave. Assuming a slit-plate of $d = 20$mm, $\nu = 0.1$ and $f = 170$Hz, we require $l_c = 0.5$m for complete absorption. This is shown in Figs. 3 (c) and (d) and Figs. 4 (c) and (d). Around $M = 0.05$, $R_L = 0$ and $\Delta_L = 1$, indicating complete absorption for 170Hz. For the same parameters, the maximum absorption attained by a slit-plate is 0.5 (Dowling and Hughes (1992)). Hence,

a cavity-backed slit-plate gives much better absorption than just a slit-plate. The effects of cavity length l_c, on $|R_L|$ and Δ_L are shown in Fig. 5 (a) and (b) respectively, for 3 frequency values : $f = 60$, 120 and 170Hz. At $l_c = 0$, the slit-plate and the backing wall are assumed to overlap, resulting in a rigid end with complete reflection ($|R_L| = 1$) and no absorption ($\Delta_L = 0$). As l_c increases, $|R_L|$ decreases from

1, attains a minimum and then increases to 1 (Fig. 5 (a)). At this second maximum point, the l_c is equal to half the wavelength of the incident wave. This alternating behaviour of decreasing and increasing $|R_L|$ continues with increasing l_c. However, Δ_L exhibits the opposite behaviour. In spite of this periodic behaviour in Δ_L, there is a wide range of l_c values with significant absorption coefficient values.

Figure 4. Reflection coefficient and absorption coefficient of slit-plate ((a) and (b)) and cavity-backed slit-plate ((c) and (d)) as a function of Frequencies, for fixed Mach numbers and $\nu = 0.1$. For (c) and (d), $l_c = 0.5$m.
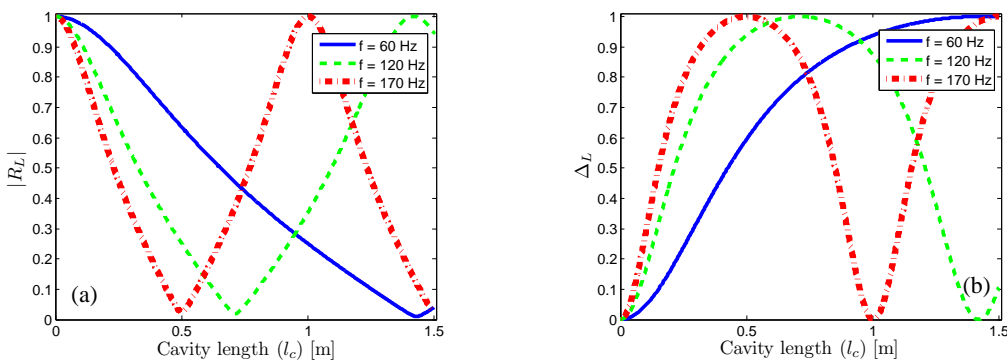
Figure 5. (a) Reflection coefficient and (b) absorption coefficients of cavity-backed slit-plate, as a function of cavity length, for fixed frequencies, $M = 0.05$ and $\nu = 0.1$.

The other parameter that helps us in controlling or varying the absorptive property of the slit-plate is the open area ratio (ν). ν is the measure of the porosity of the plate or the proportion of blockage to the incoming flow. Low values of ν indicates high blockage and vice versa. For a slit-plate with bias flow, this implies that with increasing ν values, the proportion of blockage decreases and the slit-plate becomes more '*transparent*' to the acoustic waves. Therefore, the

value of the reflection coefficient ought to decrease with increasing ν. This trend is shown in Fig. 6 (a) where $|R_{sp}|$ is plotted as a function of ν for the Mach numbers $M = 0.001$, 0.015, 0.05 and 0.1. As for the absorption, increasing ν values cause reduced interaction between the incident wave and the vortical structures downstream of the slit-plate. This causes less interaction between the incident acoustic energy and the dissipative vortices, leading to decreasing

Δ_{sp}. Figure 6 (b) shows the Δ for a slit-plate as a function of ν for M = 0.001, 0.015, 0.05 and 0.1, and we can observe the decreasing trend in Δ_{sp} for increasing ν values. Even though there is an initial increase in Δ_{sp} for small ν values, the maximum absorption achieved is only 0.5. The reflection and absorption properties of the slit-plate are greatly improved when we include the rigid backing. Figures 6 (c) and (d) show the $|R|$ and Δ of a cavity-backed slit-plate for M = 0.001, 0.015, 0.05 and 0.1, as a function of ν. It can be noted from Fig. 6 (c) that except for the lowest Mach number of 0.001, for all other M values, the $|R_L|$ decreases with increasing ν, reaches a minimum and then increases. On the other hand, Δ_L increases with increasing ν, attains a maximum of 1 and then decreases (Fig. 6 (d)). An interesting observation in the $|R_L|$ curve (Fig. 6 (c)) for the cavity-backed slit-plate is the increasing $|R_L|$ trend after attaining the minimum. But, this behaviour seems counter-intuitive when compared to the behaviour of

a slit-plates with large open area ratios. As explained earlier, increasing ν values ought to make the slit-plate *transparent* and therefore, the reflection coefficient must decrease with increasing ν values. Here, one must recall that $|R_L|$ denotes the effective reflection coefficient of the cavity-backed slit-plate, and for a '*transparent*' slit-plate backed by rigid wall, the effective reflection coefficient will tend to that of a rigid wall i.e., $|R_L| \rightarrow 1$.

In summary, for a given frequency value, the absorption efficiency of a cavity-backed slit-plate can be maximised if we choose the appropriate l_c, ν and M. In the case of a combustor with an unstable mode, the frequency of the unstable mode will be close to the eigenfrequency of the combustor. Therefore, given a fixed slit-plate dimension, we must choose the appropriate M and l_c to stabilise the combustor.
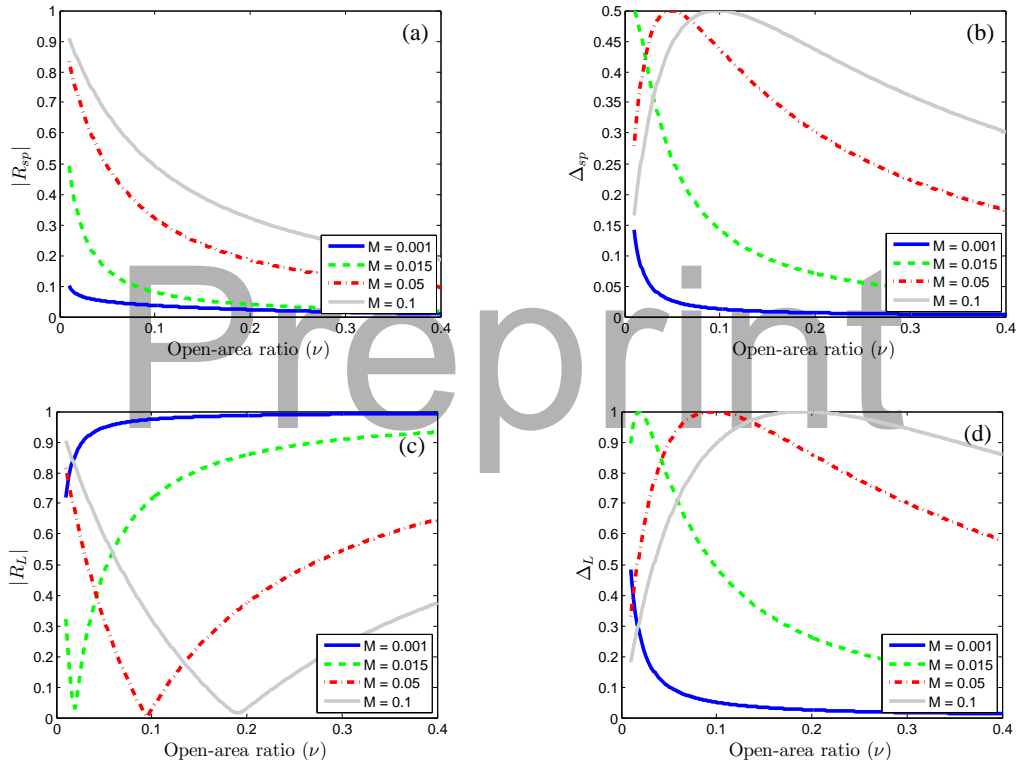
Figure 6. Reflection coefficient and absorption coefficient of slit-plate ((a) and (b)) and cavity-backed slit-plate ((c) and (d)) as a function of open area ratio, for fixed Mach numbers and f = 170Hz. For (c) and (d), l_c = 0.5m.

Stability predictions

For stability predictions, we make use of the eigenvalue method (Heckl (1985)), which is instrumental in obtaining the growth rates of different modes in the system. In the present work, we restrict ourselves to the first mode of the combustor.

Boundary and jump conditions

The unknowns in our system are the four pressure amplitudes A, B, C and D. Therefore, we need four homogeneous equations, obtained from the following boundary and jump conditions.

At $x = 0$:

$$Ae^{-ik_1 l_f} = R_0 Be^{ik_1 l_f}. \tag{14}$$

At $x = L$:

$$De^{-ik_2(L-l_f)} = R_L Ce^{ik_2(L-l_f)}. \tag{15}$$

R_0 and R_L are the reflection coefficients at $x = 0$ and $x = L$, respectively.

Across the heat source ($x = l_f$), we assume continuity of pressure,

$$A + B = C + D, \tag{16}$$

and a velocity jump generated by the heat source (Heckl (1988))

$$-\frac{(A-B)}{\rho_1 c_1} + \frac{(C-D)}{\rho_2 c_2} = \frac{(\gamma-1)}{\rho_1 c_1^2 S}\hat{Q}(l_f) \,, \qquad (17)$$

where S is the cross-sectional area of the duct and γ is the ratio of the specific heat capacities.

Eigenfrequencies and growth rates

Equations (14) - (17) can be rearranged in matrix form to yield:

$$[Y(\Omega)]\begin{bmatrix}A\\B\\C\\D\end{bmatrix} = \begin{bmatrix}0\\0\\0\\0\end{bmatrix} \,, \qquad (18)$$

with

Figure 7. Stability map, without slit-plate and bias flow

$$Y(\Omega) = \begin{bmatrix} e^{-i\frac{\Omega}{c_1}l_f} & -R_0 e^{i\frac{\Omega}{c_1}l_f} & 0 & 0 \\ 0 & 0 & R_L e^{i\frac{\Omega}{c_2}(L-l_f)} & -e^{-i\frac{\Omega}{c_2}(L-l_f)} \\ 1 & 1 & -1 & -1 \\ (-1-\beta_1 e^{i\Omega\tau}+\beta_0) & (1+\beta_1 e^{i\Omega\tau}-\beta_0) & \zeta & -\zeta \end{bmatrix} \,, \qquad (19)$$

where $\beta_{0,1} = \frac{\alpha n_{0,1}(\gamma-1)}{S\rho_1 c_1^2}$ is a quantity proportional to the coupling coefficients, and $\zeta = \frac{\rho_1 c_1}{\rho_2 c_2}$ is the ratio of the specific impedances.

Solving the characteristic equation, $\det Y(\Omega) = 0$, using the Newton Raphson or bisection method, gives us the eigenfrequencies of the system. The solution $\Omega_m = \omega_m + i\,\delta_m$, is a complex quantity where ω_m denotes the natural frequency of the mode m and δ_m its growth rate. Positive δ_m indicates instability and negative δ_m indicates stability.

Stability Maps

From Eq.(19), one can infer that the parameters which affect the stability of the combustor are: the properties of the medium inside the duct ($\rho_{1,2}$, $c_{1,2}$, $T_{1,2}$), the duct length (L), the location of the heat source (l_f), the reflection coefficients at the boundaries (R_0 and R_L), the time-lag (τ), and the heat source properties (α and $n_{0,1}$). In addition to these parameters, cavity length (l_c), slit-plate dimensions (d and ν) and bias flow Mach number (M) have an indirect influence through R_L. Here, we consider the influence of the following three parameters : cavity length, heat source location and bias flow Mach number. The cold region is assumed to be at room temperature ($T_1 = 288$ K) and the hot region is assumed to be at $T_2 = 1288$ K. The duct length L is assumed to be 1 m and the heat source properties are taken as constants: $\alpha = 120\,m^2/s^2$, $n_1 = 1.2$, $n_0 = 0.2$ and $\tau = 0.15\times 10^{-3}\,s$.

The stability maps are constructed in the cavity length (l_c) - heat source location (l_f) plane, where the *grey* regions indicate instability and the *white* regions indicate stability. Stability of the first mode of the system is determined from the sign of the growth rate, δ_1, as mentioned in the previous section. Firstly, we construct the stability map for a quarter-wave resonator containing a heat source, but without the slit-plate. In the absence of the slit-plate, an increase in cavity length (l_c) effectively adds to the duct length, L. The total
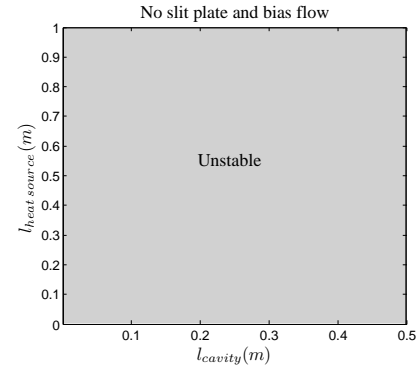
length of the resonator will now be $(L + l_c)$. As expected, the resonator is always unstable (Fig. 7), regardless of the value of l_c or the location of the heat source.

Next, we introduce a slit-plate with bias flow, into the system. The slit dimensions are $d = 0.02\,m$ and $\nu = 0.1$. Surendran and Heckl (2015) modelled a cavity-backed slit-plate with bias flow to stabilise a combustor having uniform temperature distribution ($T_1 = T_2 = 288$K) and having a heat source obeying the time-lag law ($n_1 = 1.2$, $n_0 = 0$ and $\alpha = 155.83 m^2/s^2$). The stability maps were constructed for the first mode of the combustor and for different bias flow Mach numbers. Figure 8 shows the maps for three Mach numbers, $M = 0.001$, $M = 0.005$ and $M = 0.01$. For $M = 0.001$, the stable regime of the combustor was confined to a small range of l_f and l_c values (small l_f and large l_c values). As M increased, the combustor exhibited increased stability. Figure 8 (c) shows that for a combustor of length $L = 1$m, $l_c \approx 0.15$m is sufficient to stabilise the first mode of the combustor, when $M = 0.01$. The stable regimes of the combustor can thus be extended by choosing appropriate bias flow M and l_c values. This makes the configuration of a cavity-backed slit-plate with bias flow, an effective passive instability controller.

The present study is an extension to the work by Surendran and Heckl (2015). We modified the time-lag model for heat release to a more general one that takes into account the influence of instantaneous velocity fluctuations at the heat source location and constructed stability maps (in $l_f - l_c$ plane) for the modified system, for different M values (Fig. 9). Even though the stability maps obtained for the combustor configuration with uniform temperature and generic heat release law, exhibit the trends observed by Surendran and Heckl (2015), the unstable regimes are comparatively larger, for the same M values. This is plausible because we have included additional fluctuations to our heat release and these could de-stabilise the combustor.

As a step further to our study, we also incorporated a temperature jump across the heat source (T_1 = 288K and T_2 = 1288K). The assumption of a temperature jump makes the combustor more realistic and close to real situations. The stability maps, again constructed in the l_f - l_c plane for 3 Mach numbers: M = 0.001, 0.005 and 0.01, are given

in Fig. 10. Comparison of Fig. 10 and Fig. 9 shows that having a hot region or temperature non-uniformity within the combustor tends to de-stabilise it. However, it is still possible to find a cavity length and Mach number that stabilises the combustion system.
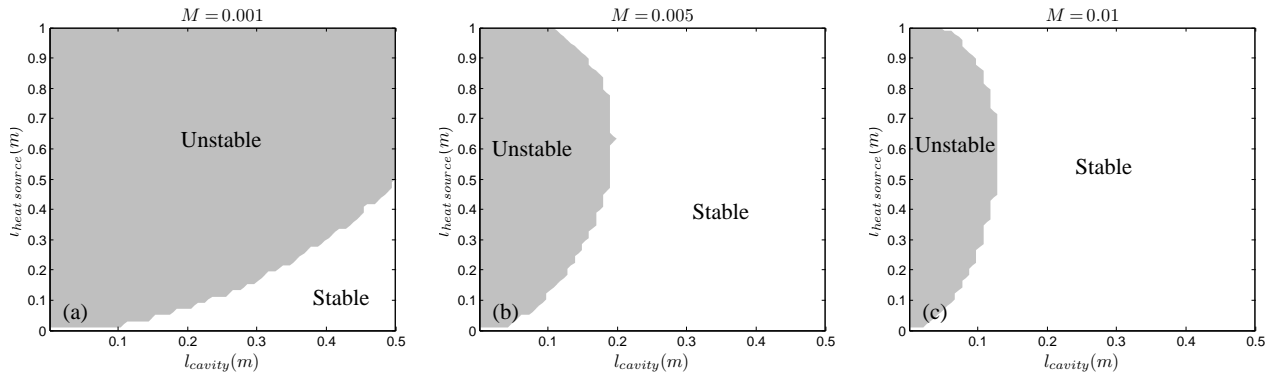
Figure 8. Stability maps for different Mach numbers (a) M = 0.001, (b) M = 0.005 and (c) M = 0.01, for a combustor with uniform temperature and time-lag model for heat release rate. Results from Surendran and Heckl (2015).
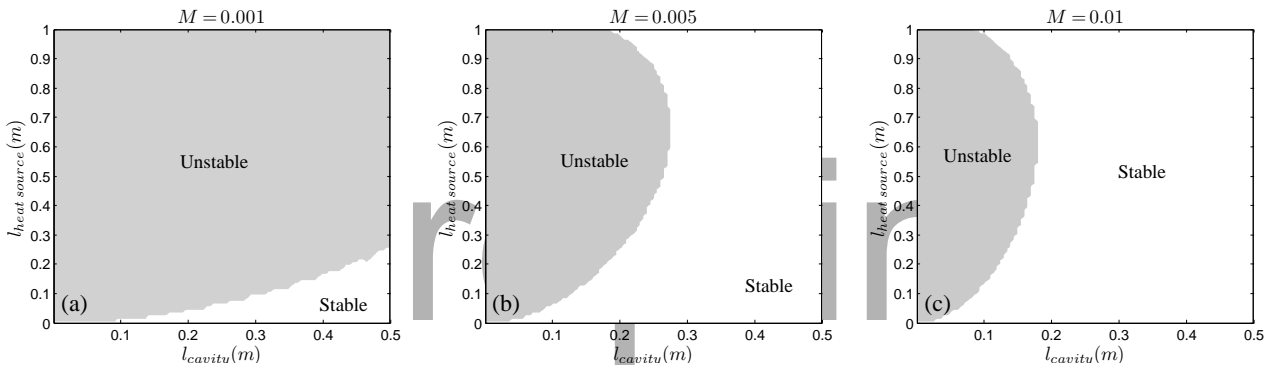
Figure 9. Stability maps for different Mach numbers (a) M = 0.001, (b) M = 0.005 and (c) M = 0.01, for a combustor with uniform temperature and a generic heat release law.
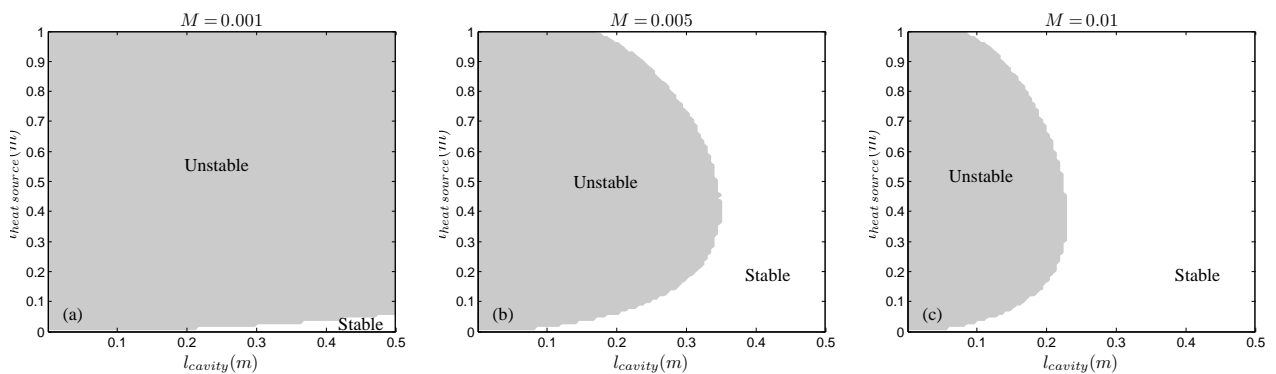
Figure 10. Stability maps for different Mach numbers (a) M = 0.001, (b) M = 0.005 and (c) M = 0.01, for a combustor with non-uniform temperature and a generic heat release law.

Summary and Outlook

Stability analysis was conducted on an existing unstable mode of a generic combustor with heat exchanger: a quarter-wave resonator with a heat source and fitted with a slit-plate near the closed downstream end. Initial observations show that the unstable mode of the combustor can be stabilised by

choosing the bias flow Mach number and the cavity length appropriately. Presently, work is in progress to identify and utilise other potential system parameters to successfully stabilise the combustor.

Acknowledgements

References

Bechert DW (1980) Sound absorption caused by vorticity shedding, demonstrated with a jet flow. *Journal of Sound and Vibration* 70(3): 389–405.

Dowling AP and Hughes IJ (1992) Sound absorption by a screen with a regular array of slits. *Journal of Sound and Vibration* 156(3): 387–405.

Heckl M and Kosztin B (2013) Analysis and control of an unstable mode in a combustor with tuneable end condition. *International Journal of Spray and Combustion Dynamics* 5(3): 243–272.

Heckl MA (1985) *Heat Sources in Acoustic Resonators*. PhD Thesis, Emmanuel College, Cambridge.

Heckl MA (1988) Active control of the noise from a Rijke tube. *Journal of Sound and Vibration* 124(1): 117–133.

Howe MS (1979) On the Theory of Unsteady High Reynolds Number Flow Through a Circular Aperture. *Proceedings of the Royal Society A: Mathematical, Physical and Engineering Sciences* 366: 205–223.

Howe MS (1998) *Acoustics of Fluid-Structure Interactions*. Cambridge University Press.

Hughes IJ and Dowling AP (1990) The absorption of sound by perforated linings. *Journal of Fluid Mechanics* 218: 299 – 335.

Surendran A and Heckl MA (2014) Analytical study of a Rijke tube with heat exchanger. In: *The 21st International Congress on Sound and Vibration*. Beijing, China.

Surendran A and Heckl MA (2015) Passive instability control by using a heat exchanger as acoustic sink. In: *The 22nd International Congress on Sound and Vibration*, July. Florence, Italy.

Tran N, Ducruix S and Schuller T (2009) Damping combustion instabilities with perforates at the premixer inlet of a swirled burner. *Proceedings of the Combustion Institute* 32(2): 2917–2924.